

Supervised Hamiltonian learning via efficient and robust quantum descent

Tian-Lun Zhao, Shi-Xin Hu, and Yi Zhang*

International Center for Quantum Materials, School of Physics, Peking University, Beijing, 100871, China

(Dated: Today)

Given the recent developments in quantum techniques, modeling the physical Hamiltonian of a target quantum many-body system is becoming an increasingly practical and vital research direction. Here, we propose an efficient quantum strategy that mingles maximum-likelihood-estimate state and supervised machine learning. Given the measurement outcomes, we optimize the target model Hamiltonian and density operator via a series of quantum descent, which we prove is negative semi-definite with respect to the negative-log-likelihood function. In addition to such optimization efficiency, supervised Hamiltonian learning respects the locality of a given quantum system, therefore, extends readily to larger systems. Compared with previous approaches, it also exhibits better accuracy and overall stability toward noises, fluctuations, and temperature ranges, which we demonstrate with various examples.

I. INTRODUCTION

Understanding the quantum states and the corresponding properties of a given quantum Hamiltonian is a crucial problem in quantum physics. Many powerful numerical and theoretical tools have been developed for such purposes and made compelling progress [1–5]. On the other hand, with the rapid experimental developments of quantum technology, e.g., near-term quantum computation [6, 7] and simulation [8–14], it is also vital to explore the inverse problem, e.g., Hamiltonian learning - optimize a model Hamiltonian characterizing a quantum system with respect to the measurement results. Given the knowledge and assumption of a target system, researchers have achieved many resounding successes modeling quantum Hamiltonians with physical pictures and phenomenological approaches [15, 16]. However, such subjective perspectives may risk biases and are commonly insufficient on detailed quantum devices. Therefore, the explorations for objective Hamiltonian learning strategies have attracted much recent attention [17–25].

There are mainly two categories of Hamiltonian-learning strategies, based upon either quantum measurements on a large number of (identical copies of) quantum states, e.g., Gibbs states or eigenstates [17–22], or initial states' time evolution dynamics [23–25], corresponding to the target quantum system. For example, given the measurements of the correlations between k -local operators acting on no more than k contiguous sites, the kernel of the resulting correlation matrix offers a candidate model Hamiltonian [17–19]. On the other hand, while established theoretically, most approaches suffer from elevated costs and limit to small systems in experiments or numerical simulations [19, 20, 26, 27]. Besides, there remains much room for improvements in stability towards noises [28] and temperature ranges [17, 20].

Supervised machine learning has witnessed rapid developments in research and applications such as image

and speech recognition [29, 30] and, more recently, in condensed matter physics [31–35]. Through supervised machine learning on a large set of training data, models like artificial neural networks (ANNs) can optimize spontaneously and learn the targets' key features that apply to more general instances. The paradigm's success may be partially attributed to the efficient training of the ANNs, whose parameters' optimizing gradients are attainable collectively via back-propagation [29].

Here, we propose a general supervised-Hamiltonian-learning protocol: given finite-temperature measurements of the target quantum system in equilibrium, we optimize the model Hamiltonian towards the maximum likelihood estimation (MLE) via step-by-step quantum descent. We show that such quantum descent, acting collectively on all presenting operators, is negative semi-definite with respect to the negative-log-likelihood function and thus provides efficient optimization similar to supervised machine learning. In addition, our strategy may take advantage of the locality of the quantum system, therefore allowing us to extend studies to larger quantum systems with tailored quantum many-body ansatzes such as Lanczos, quantum Monte Carlo (QMC), density matrix renormalization group (DMRG), and finite temperature tensor network (FTTN)[36] algorithms in suitable scenarios. We also demonstrate that supervising Hamiltonian learning is more accurate, less restrictive, and more robust against noises and broader temperature ranges. Further, we generalize our protocol to measurements on pure states, such as the ground states or eigenstates of the target quantum system. Therefore, supervised Hamiltonian learning enriches our arsenal for cutting-edge research and applications of quantum devices and experiments, such as quantum computation, quantum simulation, and quantum Boltzmann machines.

We organize the rest of the paper as follows: In Sec. II, we review the MLE context and introduce the supervised Hamiltonian learning protocol; especially, we show explicitly that the corresponding quantum descent is negative semi-definite. Via various examples in Sec. III, we demonstrate our protocol's capability, especially its robustness against noises and temperature ranges. We

* frankzhangyi@gmail.com

generalize the protocol to quantum measurements of pure states in Sec. IV and Appendix, with consistent results for exotic quantum systems such as quantum critical and topological models. We summarize our studies in Sec. V with a conclusion on our protocol's advantages (and limitations), potential applications, and future outlooks.

II. SUPERVISED HAMILTONIAN LEARNING VIA MAXIMUM LIKELIHOOD ESTIMATION AND QUANTUM GRADIENT

To start, we consider an unknown target quantum system $\hat{H}_s = \sum_j \mu_j \hat{O}_j$ in thermal equilibrium, and measurements of k -local observables $\{\hat{O}_i\}$ - operators acting non-trivially on at most k adjacent sites - on its Gibbs state $\hat{\rho}_s = \exp(-\beta \hat{H}_s) / \text{tr}[\exp(-\beta \hat{H}_s)]$, where β is the inverse temperature. Given a sufficient number N_i of measurements of \hat{O}_i , the instances of outcome o_{λ_i} , the λ_i^{th} eigenstate of \hat{O}_i , approach asymptotically:

$$k_{i,\lambda_i} = p_{i,\lambda_i} N_i = \text{tr}[\hat{\rho}_s \hat{P}_{i,\lambda_i}] N_i, \quad (1)$$

where $p_{i,\lambda_i} = k_{i,\lambda_i} / N_i$, and \hat{P}_{i,λ_i} is the corresponding projection operator to the o_{λ_i} sector. Our goal is to locate the model Hamiltonian \hat{H}_s for the quantum system, which commonly requires the presence of all \hat{H}_s 's terms in $\{\hat{O}_i\}$.

Following previous MLE analysis [37–40], the statistical weight of any given state $\hat{\rho}$ is:

$$\mathcal{L}(\hat{\rho})^{\frac{1}{N_{\text{tot}}}} \propto \prod_{i,\lambda_i} \text{tr}[\hat{\rho} \hat{P}_{i,\lambda_i}]^{\frac{k_{i,\lambda_i}}{N_{\text{tot}}}}, \quad (2)$$

upto a trivial factor, where $N_{\text{tot}} = \sum_i N_i$ is the total number of measurements. For Hamiltonian learning, we search for (the set of parameters μ_j of) the MLE Hamiltonian \hat{H} , whose MLE quantum Gibbs state $\hat{\rho}$ maximizes the likelihood function in Eq. 2. The maximum condition for Eq. 2 can be re-expressed as:

$$\begin{aligned} \hat{R}(\hat{\rho})\hat{\rho} &= \hat{\rho}, \\ \hat{R}(\hat{\rho}) &= \sum_{i,\lambda_i} \frac{k_{i,\lambda_i}}{N_{\text{tot}}} \frac{\hat{P}_{i,\lambda_i}}{\text{tr}[\hat{\rho} \hat{P}_{i,\lambda_i}]}, \end{aligned} \quad (3)$$

see the Supplemental Material for a detailed review. Solving Eq. 3 is a nonlinear and nontrivial problem. Although many algorithms have been proposed [38–40], they mostly center around the parameterization and optimization of a quantum state $\hat{\rho}$, whose cost is exponential in the system size; extracting \hat{H} from $\hat{\rho}$ further adds up to the inconvenience.

In supervised machine learning, the model parameters are optimized collectively to reduce an overall cost function step-by-step. Inspired by its success, we take an alternative stance for the Hamiltonian learning task and update the candidate Hamiltonian \hat{H}_k , i.e., the model

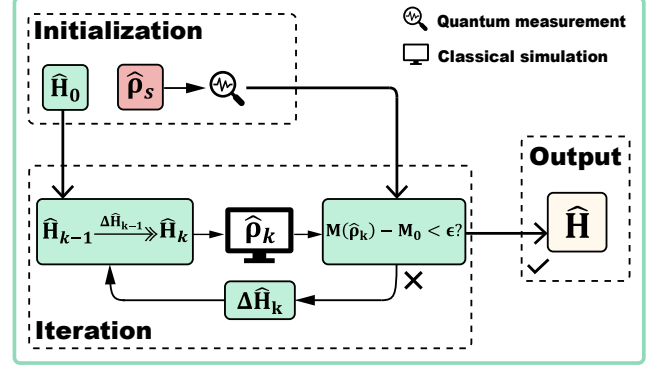


FIG. 1. An illustration of the supervised Hamiltonian learning algorithm: given the quantum measurements on the Gibbs state $\hat{\rho}_s$ of the target quantum system, we update the candidate Hamiltonian iteratively until the negative-log-likelihood function (or relative entropy) converges below a given threshold ϵ , after which the output yields the MLE Hamiltonian. Within each iterative step, we evaluate the operator expectation values with respect to the Gibbs state $\hat{\rho}_k = \exp(-\beta \hat{H}_k) / \text{tr}[\exp(-\beta \hat{H}_k)]$, which directs the model update $\Delta \hat{H}_k = -\gamma \hat{R}_k$ for the next iterative step.

parameters, collectively and iteratively. In particular, we note that $\hat{R}(\hat{\rho})$ offers such a quantum descent (Fig. 1):

$$\begin{aligned} \hat{H}_{k+1} &= \hat{H}_k - \gamma \hat{R}_k, \\ \hat{\rho}_{k+1} &= \frac{e^{-\beta \hat{H}_{k+1}}}{\text{tr}[e^{-\beta \hat{H}_{k+1}}]} = \frac{e^{-\beta(\hat{H}_k - \gamma \hat{R}_k)}}{\text{tr}[e^{-\beta(\hat{H}_k - \gamma \hat{R}_k)}]}, \end{aligned} \quad (4)$$

where $\gamma > 0$ is the learning rate - a small parameter controlling the step size. We denote $\hat{R}_k \equiv \hat{R}(\hat{\rho}_k)$ for short here afterwards. Importantly, we will show that for $\gamma \ll 1$, such a quantum descent in Eq. 4 yields a negative semi-definite contribution to the negative-log-likelihood function, guaranteeing the MLE Hamiltonian (upto a trivial constant) at its convergence and an efficient optimization toward it.

Theorem: For $\gamma \rightarrow 0$, the quantum descent in Eq. 4 yields a negative semi-definite contribution to the negative-log-likelihood function $M(\hat{\rho}) = -\frac{1}{N_{\text{tot}}} \log \mathcal{L}(\hat{\rho})$.

Proof: We note that upto linear order in $\gamma \ll 1$:

$$\begin{aligned} e^{-\beta \hat{H}_{k+1}} &= e^{-\beta \hat{H}_k} \prod_{n=0}^{\infty} \exp \left[\frac{(-1)^n}{(n+1)!} \text{ad}_{-\beta \hat{H}_k}^n (\beta \gamma \hat{R}_k) + o(\gamma^2) \right] \\ &\approx e^{-\beta \hat{H}_k} \left[1 + \sum_{n=0}^{\infty} \frac{(-1)^n}{(n+1)!} \text{ad}_{-\beta \hat{H}_k}^n (\beta \gamma \hat{R}_k) \right] \\ &= e^{-\beta \hat{H}_k} (1 + \beta \gamma \int_0^1 e^{\beta s \hat{H}_k} \hat{R}_k e^{-\beta s \hat{H}_k} ds), \end{aligned} \quad (5)$$

where $\text{ad}_A^j \hat{B} = [\hat{A}, \text{ad}_A^{j-1} \hat{B}]$ and $\text{ad}_A^0 \hat{B} = \hat{B}$ are the adjoint action of the Lie algebra. The first and third lines are based on the Zassenhaus formula and the Baker-Hausdorff formula, respectively, while the second line neglects terms above the linear order of γ .

Following this, we can re-express the quantum state in Eq. 4 as:

$$\hat{\rho}_{k+1} = \hat{\rho}_k \frac{1 + \beta\gamma \int_0^1 e^{\beta s \hat{H}_k} \hat{R}_k e^{-\beta s \hat{H}_k} ds}{1 + \beta\gamma}, \quad (6)$$

where we have used $\text{tr}[\hat{\rho}_k \hat{R}_k] = 1$ as a direct consequence of R_k 's definition in Eq. 3.

Subsequently, after the quantum descent, the negative-log-likelihood function becomes:

$$\begin{aligned} M(\hat{\rho}_{k+1}) &= -\frac{1}{N_{tot}} \log \mathcal{L}(\hat{\rho}_{k+1}) \\ &= -\sum_{i, \lambda_i} \frac{k_{i, \lambda_i}}{N_{tot}} \log \text{tr}[\hat{\rho}_{k+1} \hat{P}_{i, \lambda_i}] \\ &\approx M(\hat{\rho}_k) + \beta\gamma(1 - \Delta_k), \end{aligned} \quad (7)$$

where we keep terms upto linear order of γ in the log expansion.

On the other hand, we can establish the following inequality:

$$\begin{aligned} \Delta_k &= \text{tr}[\hat{\rho}_k \int_0^1 e^{\beta s \hat{H}_k} \hat{R}_k e^{-\beta s \hat{H}_k} \hat{R}_k ds] \\ &= \int_0^1 \text{tr}[\hat{\rho}_k e^{\beta s \hat{H}_k} \hat{R}_k e^{-\beta s \hat{H}_k} \hat{R}_k] \text{tr}[\hat{\rho}_k] ds \\ &= \int_0^1 \|e^{-\beta s \hat{H}_k/2} \hat{R}_k e^{-\beta(1-s) \hat{H}_k/2}\|_F^2 \|e^{-\beta \hat{H}_k/2}\|_F^2 \frac{ds}{Z_k^2} \\ &\geq \int_0^1 \text{tr}[\hat{\rho}_k \hat{R}_k]^2 ds = 1, \end{aligned} \quad (8)$$

where $Z_k = \text{tr}[e^{-\beta \hat{H}_k}]$ is the partition function, $\|A\|_F^2 = \text{tr}[A^\dagger A]$ is the Frobenius norm of matrix A , and the non-negative definiteness of $\hat{\rho}_k$ allows $\hat{\rho}_k = (\hat{\rho}_k^{1/2})^2 = (e^{-\beta \hat{H}_k/2})^2/Z_k$. The inequality in the fourth line follows the Cauchy-Schwarz inequality.

We note that the equal sign - the convergence criteria of our supervised-Hamiltonian-learning protocol - is established if and only if:

$$e^{-\beta s \hat{H}_k/2} \hat{R}_k e^{-\beta(1-s) \hat{H}_k/2} = e^{-\beta \hat{H}_k/2}, \quad (9)$$

which is indeed equivalent to the conventional MLE optimization target $\hat{R}\hat{\rho} = \hat{\rho}$ in Eq. 3. We can also establish such consistency from our iterative convergence [41] following Eq. 4:

$$\hat{\rho}_k \leftarrow \hat{\rho}_{k+1} = \frac{e^{-\beta(\hat{H}_k - \gamma \hat{R}_k)}}{\text{tr}[e^{-\beta(\hat{H}_k - \gamma \hat{R}_k)}]} = \frac{e^{\beta\gamma \hat{R}_k}}{\text{tr}[e^{\beta\gamma \hat{R}_k}]} \hat{\rho}_k, \quad (10)$$

where we have used the commutation relation $[\hat{R}_k, \hat{H}_k] = 0$ between the Hermitian operators \hat{R}_k and \hat{H}_k following $[\hat{R}_k, \hat{\rho}_k] = [\hat{R}_k, e^{-\beta \hat{H}_k}] = 0$.

Finally, combining Eq. 7 and Eq. 8, we have shown that $M(\hat{\rho}_{k+1}) - M(\hat{\rho}_k) \leq 0$ is a negative semi-definite quantity, which proves the theorem.

We conclude that the quantum descent in Eq. 4 offers an efficient and collective optimization towards the MLE Hamiltonian, modifying all model parameters simultaneously. For each step of quantum descent, the most costly calculation is on $\hat{\rho}_{k+1}$, or more precisely, its properties $\text{tr}[\hat{\rho}_{k+1} \hat{P}_{i, \lambda_i}]$ from \hat{H}_{k+1} . Fortunately, this is a routine calculation in quantum many-body physics and condensed matter physics with various tailored candidate algorithms under different scenarios. For example, we may resort to the FTTN, the QMC, or the minimal-entangled typical thermal state (METTS) approaches, which readily apply to much larger systems than brute-force exact diagonalization. Thus, we emphasize that supervised Hamiltonian learning works with evaluations of the expectation values of quantum states instead of the more expensive quantum states themselves in their entirety.

Interestingly, supervised Hamiltonian learning also allows a more local stance, as the necessary expectation values $\text{tr}[\hat{\rho} \hat{P}_{i, \lambda_i}]$ are local properties of a thermal system:

$$\begin{aligned} \text{tr}[\hat{\rho} \hat{P}_{i, \lambda_i}] &= \text{tr}[\hat{\rho}_{eff}^A \hat{P}_{i, \lambda_i}], \\ \hat{\rho}_{eff}^A &= \text{tr}_A[\hat{\rho}] = \frac{e^{-\beta \hat{H}_{eff}^A}}{\text{tr}[e^{-\beta \hat{H}_{eff}^A}]}, \end{aligned} \quad (11)$$

where $\hat{\rho}_{eff}^A$ is the reduced density operator defined upon a relatively local subsystem A still containing \hat{P}_{i, λ_i} . Indeed, the research on quantum belief propagation [42, 43] states that low-dimensional quantum states possess nearly Markov properties at sufficiently high temperatures, such that the effective interacting potentials $V_{eff}^A = \hat{H}_{eff}^A - \hat{H}_A$, induced by tracing out \bar{A} complementary to A , are weak and short-ranged. Therefore, we may further boost the efficiency of supervised Hamiltonian learning by redirecting the expectation-value evaluations of the global quantum system to that of a series of local patches.

In summary, given the quantum measurements of a thermal (Gibbs) state: $\{\hat{O}_i\}$, N_i , and k_{i, λ_i} , we can perform supervised Hamiltonian learning to obtain the MLE Hamiltonian via the following steps (Fig. 1):

1) Initialization/Update:

For initialization, start with a random model Hamiltonian \hat{H}_0 :

$$\hat{H}_0 = \sum_i \mu_i \hat{O}_i, \quad (12)$$

or an identity Hamiltonian.

For update, carry out the quantum descent:

$$\hat{H}_{k+1} = \hat{H}_k - \gamma \hat{R}_k, \quad (13)$$

where \hat{R}_k is defined in Eq. 3 or Eq. 16.

2) Evaluate the properties $\text{tr}[\hat{\rho}_k \hat{P}_{i, \lambda_i}]$ of the quantum state:

$$\hat{\rho}_k = \frac{e^{-\beta \hat{H}_k}}{\text{tr}[e^{-\beta \hat{H}_k}]}, \quad (14)$$

with suitable numerical methods.

- 3) Check for convergence: loop back to step 1) to update, $k \rightarrow k + 1$, if the relative entropy $M(\hat{\rho}_k) - M_0 \geq \epsilon$ is above a given threshold ϵ ; otherwise, terminate the process, and the final \hat{H}_k is the result for the MLE Hamiltonian. Here, M_0 is the theoretical minimum of the negative-log-likelihood function:

$$M_0 = - \sum_{i, \lambda_i} \frac{N_i}{N_{tot}} p_{i, \lambda_i} \log p_{i, \lambda_i}. \quad (15)$$

In practice, \hat{R}_k in Eq. 4 is singular for small values of $\text{tr}[\hat{\rho}_k \hat{P}_{i, \lambda_i}]$ and may become numerically unstable, which requires a minimal or dynamical learning rate γ to maintain the range of quantum descent properly. Instead, we may employ a re-scaled version of \hat{R}_k :

$$\tilde{R}_k = \sum_{i, \lambda_i} \frac{N_i}{N_{tot}} f_g(p_{i, \lambda_i} / \text{tr}[\hat{\rho}_k \hat{P}_{i, \lambda_i}]) \hat{P}_{i, \lambda_i}, \quad (16)$$

where f_g is a monotonic tuning-function:

$$f_g(x) = \frac{gx}{x + g - 1}, g > 1, \quad (17)$$

which maps its argument in $(0, \infty)$ to a finite range $(0, g)$. Such a re-scaled \tilde{R}_k regularizes the quantum descent and allows a simple yet relatively larger learning rate γ for more efficient supervised Hamiltonian learning. We also have $f_g(1) = 1$, therefore $\tilde{R}_k \rightarrow \hat{R}_k$ as we approach convergence. We will mainly employ \tilde{R}_k for our examples in the following sections.

In addition to the negative-log-likelihood function $M(\hat{\rho}_k)$, we also consider the Hamiltonian distance as another criterion on the quality of Hamiltonian learning:

$$\Delta \vec{\mu}_k = \frac{\|\vec{\mu}_s - \vec{\mu}_k\|_2}{\|\vec{\mu}_s\|_2}, \quad (18)$$

where $\vec{\mu}_s$ and $\vec{\mu}_k$ are the (vectors of) coefficients [44] of the target Hamiltonian and the learned Hamiltonian after k iterations, respectively. However, we do not recommend $\Delta \vec{\mu}_k$ as convergence criteria as $\vec{\mu}_s$ is generally unknown aside from benchmark scenarios [27].

III. EXAMPLE MODELS AND RESULTS

In this section, we demonstrate the performance of the supervised Hamiltonian learning protocol. In particular, we focus on general 2-local 1D quantum spin chains taking the following form:

$$\hat{H}_s = \sum_{i, \alpha, \beta}^{L-1} J_i^{\alpha\beta} \hat{S}_i^\alpha \hat{S}_{i+1}^\beta + \sum_{i, \alpha}^L h_i^\alpha \hat{S}_i^\alpha, \quad (19)$$

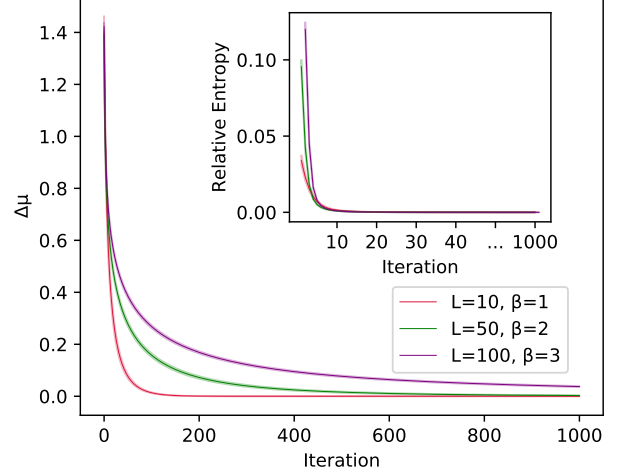


FIG. 2. Both the Hamiltonian distance $\Delta \vec{\mu}_k$ defined in Eq. 18 and the negative-log-likelihood function $M(\hat{\rho}_{k+1})$ (or relative entropy $M(\hat{\rho}_{k+1}) - M_0$) show successful convergence of the iterations in supervised Hamiltonian learning, albeit a variety of system sizes and temperature ranges. We simulate the target Hamiltonian and the iteration process by FTTN with Trotter step $\delta t = 0.1$. The shadow for each curve stands for the variance from 10 trials with random \hat{H}_0 initializations. We set the learning rate $\gamma = 1$.

where \hat{S}_i^α denotes the spin operator on site i , $\alpha, \beta \in \{x, y, z\}$. There are $12L - 9$ 2-local operators under the open boundary condition, where L is the system size. We generate the model parameters $\vec{\mu}_s = \{J_i^{\alpha\beta}, h_i^\alpha\}$ randomly following a uniform distribution in $[-1, 1]$. This Hamiltonian \hat{H}_s , specifically the model parameters $\vec{\mu}_s$, will be our target for supervised Hamiltonian learning. As the protocol's inputs, we simulate quantum measurements of all 2-local operators $\{\hat{O}_i\}$ on the Gibbs states of \hat{H}_s numerically via exact diagonalization on small systems and FTTN for large systems [36]. For the latter, we employ a tensor network (TN) ansatz called the “ancilla” method, where we purify the mixed state by some auxiliary qubits (or qudits) and thermalize the purified state by applying Trotter gates as an imaginary time evolution. We set the Trotter step $\delta t \in [0.01, 0.1]$, for which the Trotter error shows little impact on our protocol's accuracy. Without loss of generality, we hereafter set $g = 2$ for the tuning function in \tilde{R}_k , and the number of measures $N_i = N$ for all operators in our examples for simplicity.

As we demonstrate in Fig. 2, supervised Hamiltonian learning obtains the target Hamiltonians with high accuracy and efficiency under various settings of system sizes and inverse temperatures β . Not only have we achieved comparable results to previous methods [19], Hamiltonian distance $\Delta \vec{\mu}_k \sim O(10^{-9})$ and relative entropy $M(\hat{\rho}_k) - M_0 \sim O(10^{-14})$ at convergence, for $L = 10$ systems at $\beta = 1$ straightforwardly, but we have also achieved satisfactory consistency, $\Delta \vec{\mu}_k \sim O(10^{-2})$ and

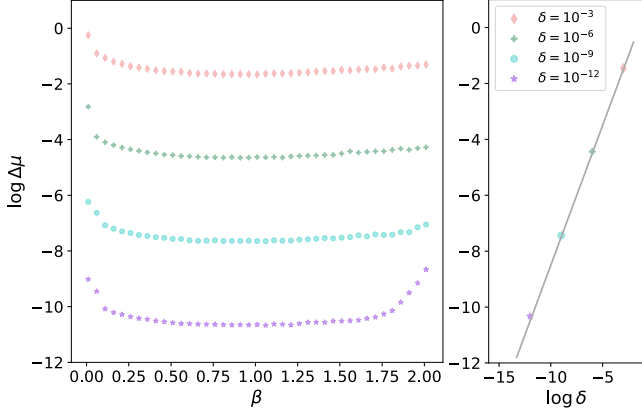


FIG. 3. The performance of supervised Hamiltonian learning maintains relatively well against noises and, especially, broader temperature ranges. Left: the Hamiltonian distance versus the inverse temperature β shows a broader applicable temperature range. Each data point contains 10 trials. Right: the performance (left figure's data averaged over temperature) versus the noise strength δ shows the impact of noises and the protocol's relative robustness against them. The slope of the straight line is ~ 1 , indicating a linear relationship between $\Delta\mu$ and δ . Note the log scale $\log(\Delta\mu)$ for the vertical axis. We set $L = 10$ for the system size, and learning rate $\gamma = 1$.

$M(\hat{\rho}_k) - M_0 \sim O(10^{-6})$ for $L = 100$ and $\beta = 3$ - large systems at low temperatures that were previously inaccessible.

Supervised Hamiltonian learning is also relatively robust against temperature and noises, two key factors impacting accuracy in Hamiltonian learning. For illustration, we include random errors $\delta\langle\hat{O}_i\rangle$ following Gaussian distribution with zero mean and standard deviation δ to all quantum measurements: $\langle\hat{O}_i\rangle \rightarrow \langle\hat{O}_i\rangle + \delta\langle\hat{O}_i\rangle$. We note that such δ may also depict the quantum fluctuations [19, 21] from a finite number of measurements $\delta \propto N_i^{-1/2}$. We also focus on smaller systems with $L = 10$ and employ exact diagonalization to avoid confusion from potential Trotter error of the FTTN ansatz. We summarize the results in Fig. 3.

Most previous algorithms on Hamiltonian learning have a rather specific applicable temperature range. For example, the high-temperature expansion of $e^{-\beta H}$ only works in the $\beta \ll 1$ limit [45, 46]. Similarly, gradient descent on the log partition function, despite a convex optimization, performs well in a narrow temperature range [20]. For example, for 2-local Hamiltonians with $L = 5$ and $\delta \propto O(10^{-3})$, a gradient-descent optimization with respect to the log partition function displays an optimal accuracy of order $O(10^{-2})$ when $0.05 < \beta < 0.65$. Indeed, supervised Hamiltonian learning retains a relatively stable performance even at larger β . In fact, our protocol is directly applicable to the ground states of quantum systems, the $\beta \rightarrow \infty$ limit, as we will generalize and justify later.

Supervised Hamiltonian learning is also more robust

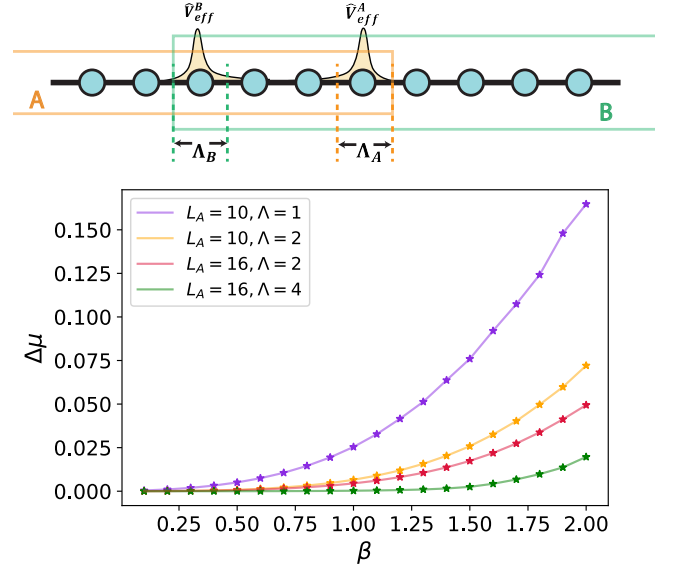


FIG. 4. Upper: supervised Hamiltonian learning's need for evaluations of local observables can be satisfied among local patches for thermal states at sufficiently high temperatures, where the effective potential V_{eff}^A (V_{eff}^B) is weak and localized on the boundaries of subregion A (B) within a cut-off range Λ_A (Λ_B). Consequently, for \hat{P}_{i,λ_i} defined sufficiently deep inside A (B), we can estimate its expectation value via $\text{tr}[\hat{\rho}^A \hat{P}_{i,\lambda_i}]$ ($\text{tr}[\hat{\rho}^B \hat{P}_{i,\lambda_i}]$). Lower: the Hamiltonian distance $\Delta\mu$ of the results after supervised Hamiltonian learning indicates better validity of the local-patch approximation at higher temperatures. The total system size is $L = 100$, while the local patches are of sizes $L_A = 10, 16$ with cut-offs $\Lambda = 1, 2, 4$, respectively. Each data point contains 10 trials. We set $\delta t = 0.1$ for the Trotter step in FTTN ansatz and learning rate $\gamma = 1$.

to noises, with an accuracy of Hamiltonian distance $\Delta\mu_k \sim O(10^{-11})$ across a broad temperature range at noise strength $\delta \sim O(10^{-12})$. Such noise level is hard to realize in practice; nevertheless, it is necessary to safeguard the correlation matrix method [17, 19, 21]. Even so, due to the uncontrollable spectral gap, the correlation matrix method is susceptible to high temperature, and its accuracy drastically decreases to $\Delta\mu_k \sim O(10^{-3})$ at $\beta = 0.01$. In comparison, supervised Hamiltonian learning is more versatile, with an approximately linear dependence between its accuracy $\Delta\mu_k$ and the noise strength δ across a broad range of temperatures and noise strengths, saturating the previous bound [20]; see the right panel of Fig. 3.

Despite efficient quantum descent and applicable quantum many-body ansatz, the computational cost of supervised Hamiltonian learning still increases rapidly with the system size L . Fortunately, as stated above in Eq.11, we may resort to calculations on local patches, especially for low dimensions and high temperatures due to their quasi-Markov property. In particular, when $\beta < \beta_c$ ($T > T_c$), the difference between \hat{H}_A and the effective Hamiltonian \hat{H}_{eff}^A in a local subregion A, V_{eff}^A , should be weak, short-

ranged, and localized at A 's boundary [42, 43]; therefore, for those \hat{P}_{i,λ_i} adequately deep inside A , we can use $\hat{\rho}^A$, the Gibbs state defined by \hat{H}_A , to estimate the corresponding $\text{tr}[\hat{\rho}^A \hat{P}_{i,\lambda_i}]$; see illustration in Fig. 4 upper panel.

For example, we apply supervised Hamiltonian learning on $L = 100$ systems, where we iteratively calculate the necessary expectation values on different local patches of size $L_A = 10, 16$. We also choose different cut-offs Λ , and evaluate $\text{tr}[\hat{\rho}^A \hat{P}_{i,\lambda_i}]$ for those operators at least Λ away from the boundaries and sufficiently deep inside the subregion A , so that the effective potential V_{eff}^A may become negligible. We also employ a sufficient number of local patches to guarantee full coverage of necessary observables - operators outside A or in Λ_A are obtainable from another local patch B , as shown in the upper panel of Fig. 4, and so on so forth. Both the $L = 100$ target system and the local patches for supervised Hamiltonian learning are simulated via FTTN. We have no problem achieving convergence, and the resulting Hamiltonians' accuracy, the Hamiltonian distance $\Delta\tilde{u}$ versus the inverse temperature β , is summarized in the lower panel of Fig. 4. Indeed, the local-patch approximation is more reliable at higher temperatures, as well as with larger subsystems and cutoffs, albeit with rising costs. We also note that we can achieve much larger systems with the local patches than $L = 100$ we have demonstrated.

IV. SUPERVISED HAMILTONIAN LEARNING FOR PURE EIGENSTATES

In addition to the Gibbs states, supervised Hamiltonian learning also applies to measurements of certain eigenstates of target quantum systems:

1. The ground states are essentially the $\beta \rightarrow \infty$ limit of the Gibbs states. However, due to the order-of-limit issue, the $\gamma \rightarrow 0$ requirement of the theorem on Gibbs states forbids a direct extension to the ground states. In the Appendix, we offer rigorous proof of the effectiveness of quantum descent based on ground-state measurements, along with several nontrivial supervised-Hamiltonian-learning examples on quantum critical and topological ground states. We note that Ref. 47 offers preliminary studies on pure-state quantum state tomography, inspiring this work.

2. A highly-excited eigenstate of a (non-integrable) quantum chaotic system \hat{H}_s is believed to obey the eigenstate thermalization hypothesis (ETH), that its density operator $\hat{\rho}_s = |\psi_s\rangle\langle\psi_s|$ behaves locally indistinguishable from a Gibbs state $\hat{\rho}_{s,A}$ in thermal equilibrium [48]:

$$\hat{\rho}_{s,A} = \text{tr}_A[\hat{\rho}_s] \approx \frac{e^{-\beta_s \hat{H}_A}}{\text{tr}[e^{-\beta_s \hat{H}_A}]}, \quad (20)$$

where β_s is an effective temperature determined by the energy expectation value $\langle\psi_s|\hat{H}_s|\psi_s\rangle = \frac{\text{tr}[e^{-\beta_s \hat{H}_s} \hat{H}_s]}{\text{tr}[e^{-\beta_s \hat{H}_s}]}$. As

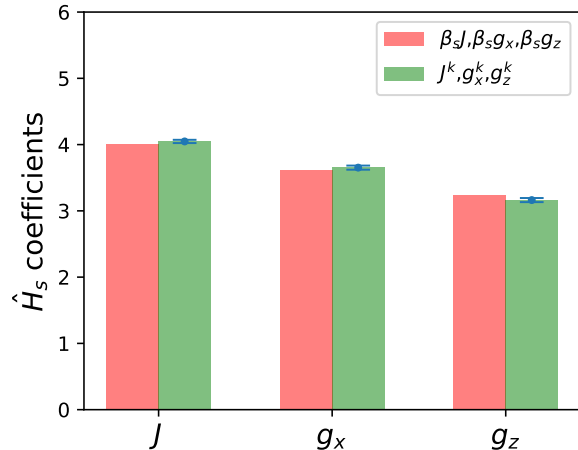


FIG. 5. The coefficients obtained via supervised Hamiltonian learning (green columns) compare well with those of the target Hamiltonian \hat{H}_s even though the quantum measurements are based upon a low-lying (first) excited state. The red columns denote the coefficients of \hat{H}_s in Eq. 21 multiply the effective (inverse) temperature $\beta_s = 4$. The error bars demonstrate the variances over the lattices and trials. We set the system size $L = 80$, learning rate $\gamma = 0.1$, and the Trotter step $\delta t = 0.1$.

supervised Hamiltonian learning only engages local operators, its applicability directly generalizes to such eigenstates $|\psi_s\rangle$ following ETH.

3. In general, ETH applies to eigenstates in the center of the spectrum of quantum chaotic systems, while low-lying eigenstates are too close to the ground state to exhibit ETH [49]. However, in the rest of the section, we demonstrate numerically that supervised Hamiltonian learning still works well for low-lying eigenstates.

We consider the 1D longitudinal-transverse-field Ising model [48, 49] as our target quantum system:

$$\hat{H}_s = J \sum_j^{L-1} \hat{\sigma}_j^z \hat{\sigma}_{j+1}^z + g_z \sum_j^L \hat{\sigma}_j^z + g_x \sum_j^L \hat{\sigma}_j^x, \quad (21)$$

where the system size is $L = 80$. We set $J = 1$, $g_x = 0.9045$, and $g_z = 0.8090$. The quantum system is strongly non-integrable under such settings. Previous studies mainly focused on eigenstates in the middle of the energy spectrum. In contrast, we pick the first excited state - a typical low-lying eigenstate considered asymptotically integrable and ETH-violating [49] - for quantum measurements (via DMRG) and then supervised Hamiltonian learning for its candidate Hamiltonian (via FTTN).

We summarize the results in Fig. 5. Further, the model Hamiltonian we established is approximately equivalent to the target quantum Hamiltonian at an (inverse) temperature $\beta_s \approx 4$ [48], which we have absorbed into the unit of our \hat{H}_k . Therefore, we have accurately

established the model Hamiltonian and derived the effective temperature consistent with previous results [48] for a low-lying excited eigenstate not necessarily following ETH. The physical reason for quantum descent's applicability in such states is an interesting problem that deserves further studies.

V. DISCUSSIONS

We have proposed a novel supervised-Hamiltonian-learning protocol to achieve the model Hamiltonian of the target quantum system based on quantum measurements of its Gibbs states. Combining supervised machine learning and MLE analysis, the protocol updates the model Hamiltonian iteratively with respect to the negative-log-likelihood function from the measurement data. We have theoretically proved the efficiency and convergence of the corresponding quantum descent and demonstrated it numerically on multiple non-trivial examples, which show more accuracy, better robustness against noises, and less temperature dependence. Indeed, the accuracy is almost linear to the imposed noise amplitude, thus inverse proportional to the square of the number of samples, the asymptotic upper bound[20]. Further, supervised Hamiltonian learning directly rests on the Hamiltonians and their physical properties instead of direct and costly access to the quantum many-body states. Consequently, we can resort to various quantum many-body ansatzes in our systematic quantum toolbox and even local-patch approximation when the situation allows. These advantages allow applications to larger systems and lower temperatures with better accuracy than previous approaches. On the other hand, while our protocol is generally applica-

ble for learning any Hamiltonian, its advantages are most apparent for local Hamiltonians, where various quantum many-body ansatzes and local-patch approximation shine. Despite such limitations, we note that the physical systems are characterized by local Hamiltonians in a significant proportion of scenarios.

In addition to the Gibbs states, we have generalized the applicability of supervised Hamiltonian learning to eigenstates of the target quantum states, including ground states, ETH states, and even selected cases of low-lying excited states. We have also provided theoretical proof of quantum descent's rigor and convergence in the Appendix, along with several other numerical examples.

Our strategy may apply to the entanglement Hamiltonians and the model Hamiltonians of the quantum states under the maximum-likelihood-maximum-entropy assumption [50]. Besides, our algorithm may also provide insights into the quantum Boltzmann machine [51] - a quantum version of the classical Boltzmann machine with degrees of freedom that obey the distribution of a target quantum Gibbs state. Instead of brute-force calculations of the loss function derivatives with respect to the model parameters or approximations with the gradients' upper bounds, our protocol provides an efficient optimization that updates the model parameters collectively.

Acknowledgement:- We thank insightful discussions with Jia-Bao Wang. We acknowledge support from the National Key R&D Program of China (No.2021YFA1401900) and the National Science Foundation of China (No.12174008 & No.92270102). The calculations of this work are supported by HPC facilities at Peking University.

-
- [1] C. Lanczos, An iteration method for the solution of the eigenvalue problem of linear differential and integral operators, *Journal of Research of the National Bureau of Standards* **45**, 255 (1950).
 - [2] S. R. White, Density matrix formulation for quantum renormalization groups, *Phys. Rev. Lett.* **69**, 2863 (1992).
 - [3] U. Schollwoeck and . B. Germany Institute for Advanced Study Berlin, Wallotstrasse 19, The density-matrix renormalization group in the age of matrix product states, *Annals of Physics (New York)* **326**, 10.1016/j.aop.2010.09.012 (2011).
 - [4] W. M. C. Foulkes, L. Mitas, R. J. Needs, and G. Rajagopal, Quantum monte carlo simulations of solids, *Rev. Mod. Phys.* **73**, 33 (2001).
 - [5] X. W. Zhang and Y. L. Liu, Electronic transport and spatial current patterns of 2d electronic system: A recursive green's function method study, *AIP Advances* **9**, 115209 (2019).
 - [6] M. A. Nielsen and I. Chuang, *Quantum computation and quantum information* (2002).
 - [7] C. Nayak, S. H. Simon, A. Stern, M. Freedman, and S. Das Sarma, Non-abelian anyons and topological quantum computation, *Rev. Mod. Phys.* **80**, 1083 (2008).
 - [8] I. Buluta and F. Nori, Quantum simulators, *Science* **326**, 108 (2009).
 - [9] I. M. Georgescu, S. Ashhab, and F. Nori, Quantum simulation, *Rev. Mod. Phys.* **86**, 153 (2014).
 - [10] P. Barthélemy and L. M. K. Vandersypen, Quantum dot systems: a versatile platform for quantum simulations, *Annalen der Physik* **525**, 808 (2013).
 - [11] A. Browaeys and T. Lahaye, Many-body physics with individually controlled rydberg atoms, *Nature Physics* **16**, 132 (2020).
 - [12] P. Scholl, M. Schuler, H. J. Williams, A. A. Eberharter, D. Barredo, K.-N. Schymik, V. Lienhard, L.-P. Henry, T. C. Lang, T. Lahaye, A. M. Läuchli, and A. Browaeys, Quantum simulation of 2d antiferromagnets with hundreds of rydberg atoms, *Nature* **595**, 233 (2021).
 - [13] S. Ebadi, A. Keesling, M. Cain, T. T. Wang, H. Levine, D. Bluvstein, G. Semeghini, A. Omran, J.-G. Liu, R. Samajdar, X.-Z. Luo, B. Nash, X. Gao, B. Barak, E. Farhi, S. Sachdev, N. Gemelke, L. Zhou, S. Choi, H. Pichler, S.-T. Wang, M. Greiner, V. Vuletić, and M. D. Lukin, Quantum optimization of maximum independent

- set using rydberg atom arrays, *Science* **376**, 1209 (2022).
- [14] D. Bluvstein, A. Omran, H. Levine, A. Keesling, G. Semeghini, S. Ebadi, T. T. Wang, A. A. Michailidis, N. Maskara, W. W. Ho, S. Choi, M. Serbyn, M. Greiner, V. Vuletić, and M. D. Lukin, Controlling quantum many-body dynamics in driven rydberg atom arrays, *Science* **371**, 1355 (2021).
 - [15] R. Bistritzer and A. H. MacDonald, Moiré bands in twisted double-layer graphene, *Proceedings of the National Academy of Sciences* **108**, 12233 (2011).
 - [16] J. Bardeen, L. N. Cooper, and J. R. Schrieffer, Theory of superconductivity, *Phys. Rev.* **108**, 1175 (1957).
 - [17] X.-L. Qi and D. Ranard, Determining a local Hamiltonian from a single eigenstate, *Quantum* **3**, 159 (2019).
 - [18] M. Dupont, N. Macé, and N. Laflorencie, From eigenstate to hamiltonian: Prospects for ergodicity and localization, *Phys. Rev. B* **100**, 134201 (2019).
 - [19] E. Baïrey, I. Arad, and N. H. Lindner, Learning a local hamiltonian from local measurements, *Phys. Rev. Lett.* **122**, 020504 (2019).
 - [20] A. Anshu, S. Arunachalam, T. Kuwahara, and M. Soleimanifar, Sample-efficient learning of interacting quantum systems, *Nature Physics* **17**, 931 (2021).
 - [21] J. Zhou and D. L. Zhou, Recovery of a generic local hamiltonian from a steady state, *Phys. Rev. A* **105**, 012615 (2022).
 - [22] X. Turkeshi, T. Mendes-Santos, G. Giudici, and M. Dalmonde, Entanglement-guided search for parent hamiltonians, *Phys. Rev. Lett.* **122**, 150606 (2019).
 - [23] A. Valenti, G. Jin, J. Léonard, S. D. Huber, and E. Greplova, Scalable hamiltonian learning for large-scale out-of-equilibrium quantum dynamics, *Phys. Rev. A* **105**, 023302 (2022).
 - [24] Z. H. X. Y. Wenjun Yu, Jinzhao Sun, Practical and efficient hamiltonian learning (2022), arXiv:2201.00190.
 - [25] D. F. Y. S. Hsin-Yuan Huang, Yu Tong, Learning many-body hamiltonians with heisenberg-limited scaling (2022), arXiv:2210.03030.
 - [26] J. Wang, S. Paesani, R. Santagati, S. Knauer, A. A. Gentile, N. Wiebe, M. Petruzzella, J. L. O'Brien, J. G. Rarity, A. Laing, and M. G. Thompson, Experimental quantum hamiltonian learning, *Nature Physics* **13**, 551 (2017).
 - [27] J. Carrasco, A. Elben, C. Kokail, B. Kraus, and P. Zoller, Theoretical and experimental perspectives of quantum verification, *PRX Quantum* **2**, 010102 (2021).
 - [28] I. R. D. H. R. S. J. E. Frederik Wilde, Augustine Kshetrimayum, Scalably learning quantum many-body hamiltonians from dynamical data (2022), arXiv:2209.14328.
 - [29] Michael A. Nielsen, *Neural Networks and Deep Learning* (Determination Press, 2015).
 - [30] M. Jordan and T. Mitchell, Machine learning: Trends, perspectives, and prospects, *Science* **349**, 255 (2015).
 - [31] J. Carrasquilla and R. G. Melko, Machine learning phases of matter, *Nature Physics* **13**, 431 (2017).
 - [32] Y. Zhang and E.-A. Kim, Quantum Loop Topography for Machine Learning, *Phys. Rev. Lett.* **118**, 216401 (2017).
 - [33] K. Ch'ng, J. Carrasquilla, R. G. Melko, and E. Khatami, Machine Learning Phases of Strongly Correlated Fermions, *Phys. Rev. X* **7**, 031038 (2017).
 - [34] P. Zhang, H. Shen, and H. Zhai, Machine learning topological invariants with neural networks, *Phys. Rev. Lett.* **120**, 066401 (2018).
 - [35] Y. Zhang, A. Mesaros, K. Fujita, S. Edkins, M. Hamidian, K. Ch'ng, H. Eisaki, S. Uchida, J. S. Davis, E. Khatami, *et al.*, Machine learning in electronic-quantum-matter imaging experiments, *Nature* **570**, 484 (2019).
 - [36] A. E. Feiguin and S. R. White, Finite-temperature density matrix renormalization using an enlarged hilbert space, *Phys. Rev. B* **72**, 220401 (2005).
 - [37] Z. Hradil, Quantum-state estimation, *Phys. Rev. A* **55**, R1561 (1997).
 - [38] J. Řeháček, Z. c. v. Hradil, E. Knill, and A. I. Lvovsky, Diluted maximum-likelihood algorithm for quantum tomography, *Phys. Rev. A* **75**, 042108 (2007).
 - [39] A. I. Lvovsky, Iterative maximum-likelihood reconstruction in quantum homodyne tomography, *Journal of Optics B: Quantum and Semiclassical Optics* **6**, S556 (2004).
 - [40] Y. S. Teo, B. Stoklasa, B.-G. Englert, J. Řeháček, and Z. c. v. Hradil, Incomplete quantum state estimation: A comprehensive study, *Phys. Rev. A* **85**, 042317 (2012).
 - [41] In practice, given sufficient measurements, we have $\hat{R}_k \sim \hat{I}$ dictating the quantum descent at the iteration's convergence.
 - [42] E. Bilgin and D. Poulin, Coarse-grained belief propagation for simulation of interacting quantum systems at all temperatures, *Phys. Rev. B* **81**, 054106 (2010).
 - [43] T. Kuwahara, K. Kato, and F. G. S. L. Brandão, Clustering of conditional mutual information for quantum gibbs states above a threshold temperature, *Phys. Rev. Lett.* **124**, 220601 (2020).
 - [44] We typically perform supervised Hamiltonian learning and update the model Hamiltonian on the projection-operator basis; therefore, we transform the Hamiltonian back to the original, ordinary operator basis before $\Delta\vec{\mu}_k$ evaluations.
 - [45] E. T. Jeongwan Haah, Robin Kothari, Optimal learning of quantum hamiltonians from high-temperature gibbs states (2021), arXiv:2108.04842.
 - [46] K. Rudinger and R. Joynt, Compressed sensing for hamiltonian reconstruction, *Phys. Rev. A* **92**, 052322 (2015).
 - [47] Y. Z. Jia-Bao Wang, Single-shot quantum measurements sketch quantum many-body states (2022), arXiv:2203.01348.
 - [48] J. R. Garrison and T. Grover, Does a single eigenstate encode the full hamiltonian?, *Phys. Rev. X* **8**, 021026 (2018).
 - [49] H. Kim, T. N. Ikeda, and D. A. Huse, Testing whether all eigenstates obey the eigenstate thermalization hypothesis, *Phys. Rev. E* **90**, 052105 (2014).
 - [50] Y. S. Teo, H. Zhu, B.-G. Englert, J. Řeháček, and Z. c. v. Hradil, Quantum-state reconstruction by maximizing likelihood and entropy, *Phys. Rev. Lett.* **107**, 020404 (2011).
 - [51] M. H. Amin, E. Andriyash, J. Rolfe, B. Kulchytskyy, and R. Melko, Quantum boltzmann machine, *Phys. Rev. X* **8**, 021050 (2018).
 - [52] Z. Hradil, Quantum-state estimation, *Phys. Rev. A* **55**, R1561 (1997).
 - [53] A. Rahmani, X. Zhu, M. Franz, and I. Affleck, Phase diagram of the interacting majorana chain model, *Phys. Rev. B* **92**, 235123 (2015).
 - [54] S.-S. Gong, W. Zhu, J.-X. Zhu, D. N. Sheng, and K. Yang, Global phase diagram and quantum spin liquids in a spin- $\frac{1}{2}$ triangular antiferromagnet, *Phys. Rev. B* **96**, 075116 (2017).
 - [55] Y. Zhang, T. Grover, A. Turner, M. Oshikawa, and

A. Vishwanath, Quasiparticle statistics and braiding from ground-state entanglement, Phys. Rev. B **85**, 235151 (2012).

Appendix A: Maximum condition for MLE

In this appendix, we review the derivation of the maximum condition [52] in Eq. 3 in the main text.

A general quantum state takes the form of a density operator:

$$\hat{\rho} = \sum_j p_j |\psi_j\rangle \langle \psi_j|, \quad (\text{A1})$$

where $p_j \geq 0$, $\sum_j p_j = 1$, and $|\psi_j\rangle$ is a set of orthonormal basis. The search for the quantum state that maximizes the likelihood function:

$$\mathcal{L}(\hat{\rho})^{\frac{1}{N_{tot}}} = \prod_{i, \lambda_i} \text{tr}[\hat{\rho} \hat{P}_{i, \lambda_i}]^{\frac{k_{i, \lambda_i}}{N_{tot}}}, \quad (\text{A2})$$

can be converted to the optimization problem:

$$\begin{aligned} \min_{\hat{\rho} \in \mathcal{D}} \quad & M(\hat{\rho}) = -\frac{1}{N_{tot}} \log[\mathcal{L}(\hat{\rho})] \\ \text{subject to} \quad & \hat{\rho} \succeq 0, \text{tr}[\hat{\rho}] = 1. \end{aligned} \quad (\text{A3})$$

We can re-express Eq. A3 via the Lagrangian multiplier method:

$$\frac{\partial}{\partial \langle \psi_j |} \{M(\hat{\rho}) + \lambda \text{tr}[\hat{\rho}]\} = 0, \quad (\text{A4})$$

where λ is a Lagrangian multiplier. Given Eq. A1, we obtain the following solution:

$$\begin{aligned} \hat{R} |\psi_j\rangle &= |\psi_j\rangle \\ \hat{R} &= \sum_{i, \lambda_i} \frac{k_{i, \lambda_i}}{N_{tot}} \frac{\hat{P}_{i, \lambda_i}}{\text{tr}[\hat{\rho} \hat{P}_{i, \lambda_i}]}, \end{aligned} \quad (\text{A5})$$

and $\lambda = 1$. Combining Eq. A1 and Eq. A5, we obtain the maximum condition:

$$\hat{R} \hat{\rho} = \hat{\rho}. \quad (\text{A6})$$

This conclusion applies to any quantum state, not just the Gibbs state. According to the maximum entropy principle[50], we can always define an estimator as a Gibbs state to approach the above extremal condition.

Appendix B: Hamiltonian learning from ground state

In this appendix, we prove the effectiveness of quantum descent based on measurements of the target quantum system's ground state and provide several nontrivial numerical examples, including 1D critical states and 2D topological states.

1. Proof for ground-state-based quantum descent

Given a sufficient number N_i measurements of the operator \hat{O}_i on the non-degenerate ground state $|\psi_s\rangle$ of a target system \hat{H}_s , we obtain a number of outcomes as the λ_i^{th} eigenvalue of \hat{O}_i as:

$$k_{i,\lambda_i} = p_{i,\lambda_i} N_i = \langle \psi_s | \hat{P}_{i,\lambda_i} | \psi_s \rangle N_i, \quad (B1)$$

where \hat{P}_{i,λ_i} is the projection operator of the eigenvalue o_{λ_i} .

Our supervised Hamiltonian learning follows the iterations:

$$\begin{aligned} \hat{H}_{k+1} &= \hat{H}_k - \gamma \hat{R}_k, \\ \hat{R}_k &= \sum_{i,\lambda_i} \frac{k_{i,\lambda_i}}{N_{tot}} \frac{\hat{P}_{i,\lambda_i}}{\langle \psi_k^{gs} | \hat{P}_{i,\lambda_i} | \psi_k^{gs} \rangle}, \end{aligned} \quad (B2)$$

where $|\psi_k^{gs}\rangle$ is the non-degenerate ground state of \hat{H}_k .

Theorem: For $\gamma \rightarrow 0$, the quantum descent in Eq. B2 yields a negative semi-definite contribution to the negative-log-likelihood function $M(\hat{\rho}) = -\frac{1}{N_{tot}} \log \mathcal{L}(\hat{\rho})$ following Eq. 2 in the main text.

Proof: At the linear order in γ , we may treat the addition of $-\gamma \hat{R}_k$ to \hat{H}_k at the k^{th} iteration as a perturbation:

$$|\psi_{k+1}^{gs}\rangle = |\psi_k^{gs}\rangle - \gamma \hat{G}_k \hat{R}_k |\psi_k^{gs}\rangle + O(\gamma^2), \quad (B3)$$

where \hat{G}_k is the Green's function in the k^{th} iteration:

$$\hat{G}_k = \hat{Q}_k \frac{1}{E_k^{gs} - \hat{H}_k} \hat{Q}_k, \quad (B4)$$

$\hat{Q}_k = I - |\psi_k^{gs}\rangle \langle \psi_k^{gs}|$ is the projection operator orthogonal to the ground space $|\psi_k^{gs}\rangle$. E_k^{gs} is the ground-state energy. Keeping terms up to the linear order of γ in the log expansion of the negative-log-likelihood function, we have:

$$\begin{aligned} M(|\psi_{k+1}^{gs}\rangle) &= -\frac{1}{N_{tot}} \log \mathcal{L}(|\psi_{k+1}^{gs}\rangle) \\ &= -\sum_{i,\lambda_i} \frac{k_{i,\lambda_i}}{N_{tot}} \log \langle \psi_{k+1}^{gs} | \hat{P}_{i,\lambda_i} | \psi_{k+1}^{gs} \rangle, \quad (B5) \\ &\approx M(|\psi_k^{gs}\rangle) + 2\gamma \Delta_k. \end{aligned}$$

where difference takes the form:

$$\begin{aligned} \Delta_k &= \langle \psi_k^{gs} | \hat{R}_k \hat{G}_k \hat{R}_k | \psi_k^{gs} \rangle \\ &= \sum_{l \neq gs} \frac{|\langle \psi_k^{gs} | \hat{R}_k | \psi_k^l \rangle|^2}{E_k^{gs} - E_k^l} \leq 0. \end{aligned} \quad (B6)$$

Here, $E_k^l > E_k^{gs}$ because E_k^l denotes the energy for eigenstates other than the ground state. Our iteration converges when the equality in Eq. B6 is established. This happens when $|\psi_k^{gs}\rangle$ is an eigenstate of \hat{R}_k , consistent with the MLE condition $\hat{R}|\psi\rangle = |\psi\rangle$.

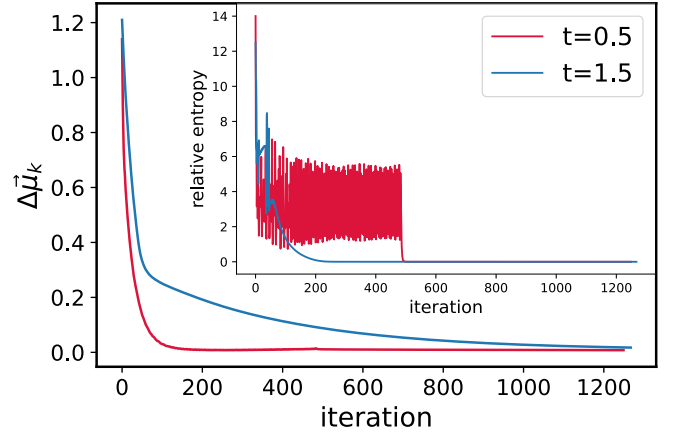


FIG. 6. Both the Hamiltonian distance $\Delta\vec{\mu}_k$ and the relative entropy $M(\hat{\rho}_{k+1}) - M_0$ (inset) as defined in the main text indicate successful convergence of the iterations during supervised Hamiltonian learning. We set $g = -1$, $t = 0.5$ (red curve) or $t = 1.5$ (blue curve), and system size $L = 12$ for the target quantum system, and learning rate $\gamma = 0.1$ ($\gamma = 0.05$) before (after) the 490th iteration.

Finally, combining Eq. B5 and Eq. B6, we have shown that $M(|\psi_{k+1}^{gs}\rangle) - M(|\psi_k^{gs}\rangle)$ is a negative semi-definite quantity, which proves the theorem.

One potential complication to the proof is that Eq. B3 needs to assume there is no ground-state level crossing or degeneracy during the quantum descent. A potential remedy is to keep some low-lying excited states together with the ground state and compare them for maximum likelihood, especially for steps with singular behaviors. Otherwise, we can only hope such transitions are sparse, especially near convergence, and they establish a new line of iterations heading toward the same convergence. A more detailed discussion is available in Ref. 47.

2. Example: $c = \frac{3}{2}$ CFT ground state of Majorana fermion chain

Here, we consider the spinless 1D Majorana fermion chain model of length $2L$ as an example [53]:

$$\hat{H}_s = \sum_j it\hat{\gamma}_j\hat{\gamma}_{j+1} + g\hat{\gamma}_j\hat{\gamma}_{j+1}\hat{\gamma}_{j+2}\hat{\gamma}_{j+3}, \quad (B7)$$

where $\hat{\gamma}_j$ is the Majorana fermion operator obeying:

$$\hat{\gamma}_j^\dagger = \hat{\gamma}_j, \{\hat{\gamma}_i, \hat{\gamma}_j\} = \delta_{ij}, \quad (B8)$$

and t and $g = -1$ are model parameters. This model presents a wealth of nontrivial quantum phases under different t/g . We focus on the model parameters in $t/g \in (-2.86, -0.28)$, where the ground state of Eq. B7 is a $c = \frac{3}{2}$ CFT composed of a critical Ising theory ($c = \frac{1}{2}$) and a Luttinger liquid ($c = 1$).

Through the definition of the complex fermions followed by the Jordan-Wigner transformation:

$$\begin{aligned}\hat{c}_j &= \frac{\hat{\gamma}_{2j} + i\hat{\gamma}_{2j+1}}{2}, \\ \hat{\sigma}_j^z &= 2\hat{n}_j - 1, \\ \hat{\sigma}_j^+ &= e^{-i\pi \sum_{i<j} \hat{n}_i} \hat{c}_j^\dagger,\end{aligned}\quad (\text{B9})$$

where $\hat{n}_j = \hat{c}_j^\dagger \hat{c}_j$ is the complex fermion number operator, we map Eq. B7 to a 3-local spin chain of length L :

$$\begin{aligned}\hat{H}_s &= t \sum_j \hat{\sigma}_j^z - t \sum_j \hat{\sigma}_i^x \hat{\sigma}_{i+1}^x \\ &\quad - g \sum_j \hat{\sigma}_i^z \hat{\sigma}_{i+1}^z - g \sum_j \hat{\sigma}_i^x \hat{\sigma}_{i+2}^x.\end{aligned}\quad (\text{B10})$$

We employ quantum measurements on the ground state $|\psi_s\rangle$ of this Hamiltonian, based on which we carry out our supervised Hamiltonian learning protocol. Here, we evaluate the ground-state properties via exact diagonalization. The numerical results for two cases of $t = 0.5, 1.5$ are in Fig. 6. We achieve successful convergence and satisfactory accuracy on the target Hamiltonian. The relative entropy's instabilities are mainly due to the ground state's level crossing and degeneracy.

3. Example: alternative Hamiltonian for ground state

We have seen that supervised Hamiltonian learning can retrieve the unknown target Hamiltonians via quantum measurements of its Gibbs states, even its ground states. For pure states, however, one interesting byproduct is that the relation between Hamiltonian and eigenstates is essentially many-to-one. Therefore, it is possible to obtain various candidate Hamiltonians \hat{H}_k sharing the same ground state as the original target \hat{H}_s , especially by controlling the operator/observable set. Here, we show such numerical examples.

As our target quantum system, we consider the transverse field Ising model (TFIM) of length $L = 15$:

$$\hat{H}_s = J \sum_j \hat{S}_j^z \hat{S}_{j+1}^z + g \sum_j \hat{S}_j^x, \quad (\text{B11})$$

at its critical point $J = g = 1$. Its ground state is $|\psi_s\rangle$. However, instead of the operators presenting in \hat{H}_s , we employ a different operator set for $|\psi_s\rangle$'s quantum measurements:

$$\{\hat{O}_i\} = \{\hat{S}_i^z \hat{S}_{i+1}^z, \hat{S}_i^x \hat{S}_{i+1}^x\}. \quad (\text{B12})$$

We evaluate the ground-state properties via DMRG.

The subsequent supervised Hamiltonian learning results are in Fig. 7. Since we obtain a candidate Hamiltonian with the operators in Eq. B12 and destined to differ from \hat{H}_s , the Hamiltonian distance is no longer a

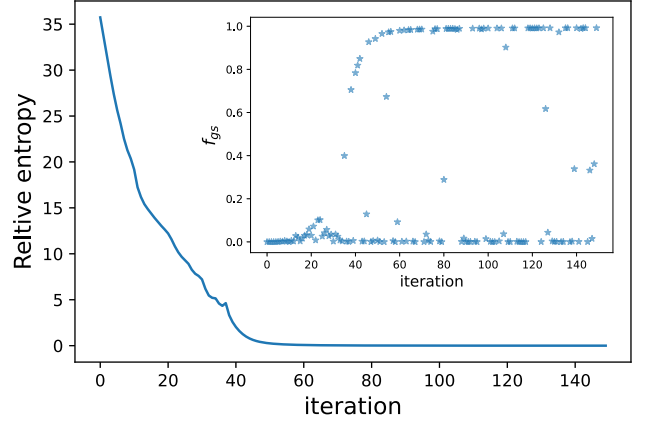


FIG. 7. Both the relative entropy and the fidelity $f_{gs} = \langle \psi_s | \psi_k^{gs} \rangle$ (inset) indicate successful convergence of the iterations during supervised Hamiltonian learning, yielding a consistent yet different Hamiltonian from the original quantum system. We set the system size $L = 15$ and learning rate $\gamma = 0.005$.

viable measure of its accuracy. Instead, we introduce the ground-state fidelity $f_{gs} = \langle \psi_s | \psi_k^{gs} \rangle$, where $|\psi_s\rangle$ ($|\psi_k^{gs}\rangle$) is the ground state of \hat{H}_s (\hat{H}_k). Interestingly, while the relative entropy shows full convergence, the fidelity f_{gs} jumps between $\sim 99.5\%$ and $\sim 10^{-3}\%$. This is understandable, as the quantum system is gapless, and the ground and low-lying excited states have similar properties under quantum measurements.

4. Example: two-dimensional topological states

Here, we consider supervised Hamiltonian learning on two-dimensional topological quantum systems. In particular, we consider the chiral spin liquid (CSL) on a triangular lattice:

$$\hat{H}_s = J_1 \sum_{\langle ij \rangle} \vec{S}_i \cdot \vec{S}_j + J_2 \sum_{\langle\langle ij \rangle\rangle} \vec{S}_i \cdot \vec{S}_j + K \sum_{i,j,k \in \nabla/\Delta} \vec{S}_i \cdot (\vec{S}_j \times \vec{S}_k), \quad (\text{B13})$$

where the first and second terms are Heisenberg interactions, and the last term is a three-spin chiral interaction. Previous DMRG studies have established \hat{H}_s 's ground state as a CSL under the model parameters $J_1 = 1.0$, $J_2 = 0.1$, and $K = 0.2$ [54], which we set as the parameters of the target Hamiltonian. Here, we employ exact diagonalization on a 4×4 system. Based upon entanglement studies of the lowest-energy eigenstates, we verify that both the modular SU matrix corresponding to C_6 rotations and the entanglement entropy fit well with a CSL topological phase[55]. Subsequently, we perform supervised Hamiltonian learning based on quantum measurements of the ground state, focusing on the operators presenting in \hat{H}_s . We summarize the results in Fig. 8. The Hamiltonian distance indicates a stable con-

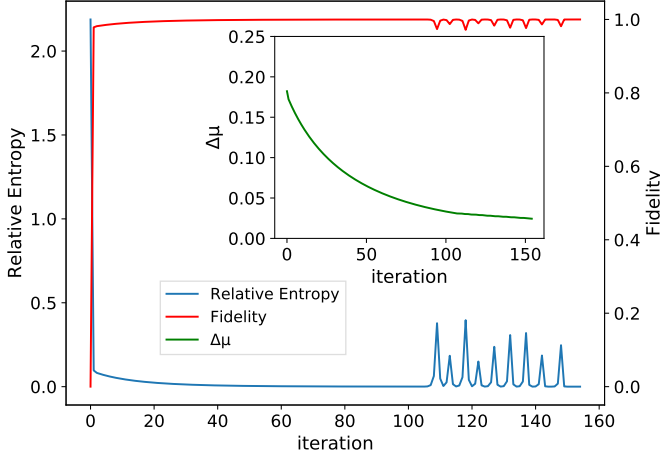


FIG. 8. The relative entropy, the fidelity $f_{gs} = \langle \psi_s | \psi_k^{gs} \rangle$, and the Hamiltonian distance $\Delta \vec{\mu}_k$ (inset) show distinct convergence behaviors in the iterations of supervised Hamiltonian learning for a 2D topological CSL system. Our system size is 4×4 , and we set the learning rate $\gamma = 0.1$.

verging accuracy, yet the relative entropy and the fidelity $f_{gs} = \langle \psi_s | \psi_k^{gs} \rangle$ witness certain instabilities. $|\psi_s\rangle$ ($|\psi_k^{gs}\rangle$) is the ground state of \hat{H}_s (\hat{H}_k). Indeed, being a topological phase means ground-state degeneracy - competing low-energy eigenstates with global distinctions yet similar local properties.